# FLUID DYNAMIC DESIGN AND OPTIMIZATION OF A DOUBLE ENTRY FAN DRIVEN BY TRACTOR POWER TAKE OFF FOR MIST SPRAYER APPLICATIONS

Michele PINELLI[1], Cristian FERRARI[1], Alessio SUMAN[1]
Mirko MORINI[2], Mauro ROSSINI[3]

[1]*Dipartimento di Ingegneria, Università di Ferrara, Ferrara, Italy*
[2]*MechLav, Università di Ferrara, Ferrara, Italy*
[3]*Ideal srl, Castelbaldo (PD), Italy*

## SUMMARY

In this paper, the fluid dynamic design of a double entry fan driven by tractor power take off for mist sprayer applications is presented. The design is carried out by means of an integrated 1D/3D numerical procedure based on the use of CFD simulations. Moreover, an experimental campaign performed to characterize the existent fans is presented. The collected data are elaborated in order to fix a design starting point and to validate the CFD procedure. The CFD simulations are then used either at the preliminary design stage to choose among competitive one- or two-dimensional geometries and then to test the generated three-dimensional geometries. The results show how the different design choices could impact on the performance parameters and, finally, how the analysis of the various alternatives allows the determination of the overall geometry of a complete and performing centrifugal fan. Finally, the double entry fan has been prototyped and tested. The test confirmed that the designed fan met the manufacture requests in terms of efficiency, maximum flow rate and head.

## INTRODUCTION

Increasing public concern about the potential damage of chemical inputs in agricultural production systems has challenged industry to develop new and effective pest management and control strategies. In conventional agriculture, effective and efficient application of biopesticides that are environmentally safe and pose no hazard to non-target organisms is dependent on the development of both the formulations and the delivery systems to ensure adequate handling, metering, dispersal and crucially, deposition of sufficient amounts of the biopesticide where the pests are located [1].

Blower or fan-assisted mist sprayers are commonly used for the distribution of herbicides, pesticides and fertilizers. Moreover, they are applied in vector control, i.e. methods to limit or eradicate insects or other arthropods that can transmit disease pathogens [2]. In particular, truck-mounted mist sprayers are used to spray insecticides to trees, shrubs, and tall grass in rural areas and to road borders and courtyards in urban areas. In practice, mist sprayer systems are designed

and commercialized in compact assembly, in order to achieve a minimal amount of occupied space and an easy and rapid load/unload procedure. These compact systems (see Fig. 1) are usually made up of: (i) a driving engine, which drives the fan and the pump for the atomizers, (ii) a fan, which provides the air for spreading the liquid droplets, (iii) a pump and the nozzles for the atomization of the liquid mixture (e.g. insecticide and water), (iv) a cannon, which directs the mist spray towards the target and (v) spray distributor to correctly scatter the product to target.

The fans used in these applications are usually connected to the power take-off of the truck, which, in turn, it is driven by the truck engine by means of a speed-up gear box. The study of these configurations can be more difficult compared to usual fan design since it is not possible to *a priori* define the operating point. In fact, the rotational speed is not fixed as in the case of an electric motor driven fan, but is determined as an equilibrium of the power supplied by the engine and the power absorbed by the fan to recover the pressure drops of the mist sprayer system. Recently, in Bettocchi *et al.* [3] the coupling of a sirocco fan, used to supply air to a mist sprayer, and a Diesel engine is studied in order to enhance the performance of the integrated system.

Mist sprayer manufacturers have shown a growing attention also as what concern fan geometry optimization, in order to achieve as high as possible performances in terms of head, achievable maximum flow rate and efficiency, while containing overall machine dimensions, energy consumption and noise. This target is truly challenging or impossible to reach since it requires to over-constraint the fan design and, thus, it is very difficult to define a geometry, which can satisfy all the requirements. More complex than usual fan geometries (such as multi-stage or double entry) can offer some advantage with respect to simple ones, but their design requires accurate aerodynamic design of both impeller and volute and a careful aerodynamic matching between them [4]. Ng and Damodaran [5] describes a CFD analysis of both a single inlet and double inlet centrifugal fan for operational conditions specified by an industry vendor aimed at the achievement of optimal fan performance characteristics. Lee *et al.* [6] a systematic numerical study of the aerodynamic characteristics of the impellers used in double-entry centrifugal fan is carried out. A detailed study of the coupled impeller-volute system was also carried out.

In this paper, the fluid dynamic design and optimization of a two-double entry centrifugal fan for mist sprayer applications is presented. The design is carried out by means of an integrated 1D/3D numerical procedure based on the use of CFD simulations. CFD has demonstrated to be a powerful tool also for the optimization of fans, which, up until now, was less utilized for this kind of machines.

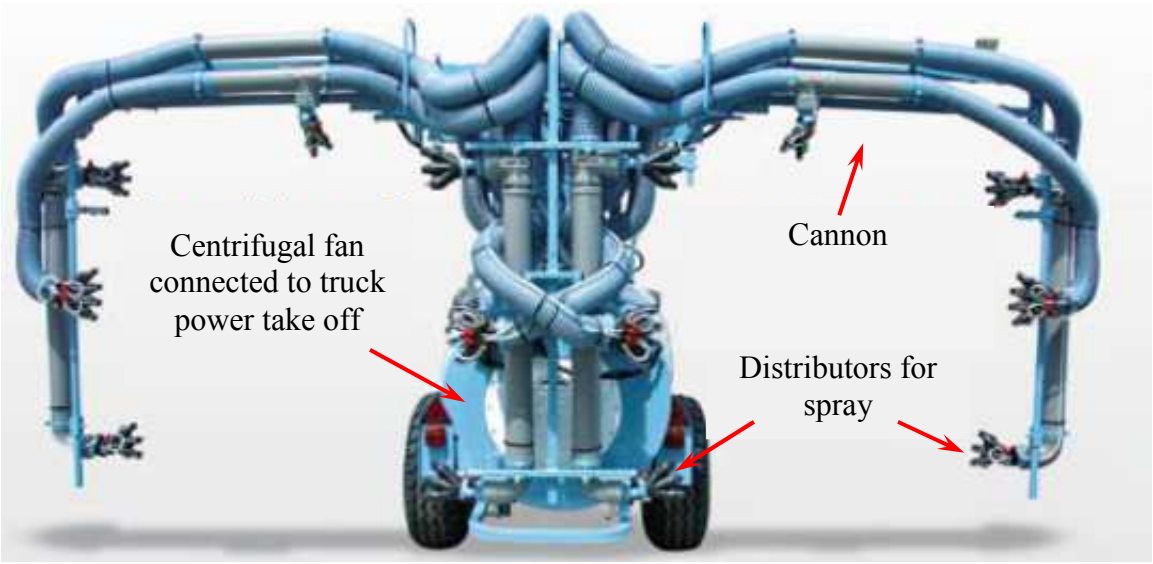


*Figure 1 - Mist sprayer (courtesy of Ideal srl)*

Comprehensive information on the use of CFD in centrifugal fan optimization can be found in [7]. In recent works, examples of advanced use of CFD regarding optimization of industrial centrifugal fans can be found in [4]. In this paper, in order to perform the design of the fan, three main phases can be recognized:

- definition of the required performances and of the geometrical constraint and one-dimensional design. Starting from the required performances, the main characteristics of machine geometry are obtained, which are: the main dimensions (diameters, flow passage areas, etc.) and the blade mean line, which has to be defined in terms of shape along the impeller and of inlet and outlet angles. The impeller blade mean line and the inlet and outlet blade angles are determined with 1D criteria according to machine specifications;
- preliminary simplified 3D simulations to choose among competitive one- or two-dimensional geometries. In this manner, a wide number of alternatives can be rapidly evaluated
- three-dimensional fluid dynamic numerical design. In this phase, the best alternatives identified in the previous phase are fully simulated and the three-dimensional geometry is optimized.

## ONE-DIMENSIONAL DESIGN

The fan to be designed is used in a mist sprayer for agricultural applications. The fan must provide the necessary air flow rate for the atomization process and must be able to overcome the pressure losses along its path. In particular, the main sources of losses are due to the cannon and to the atomizers. The fan design was part of a research project carried out in collaboration with the manufacturer, which specified the requested operating condition and the desired economic and geometric constraints. The target conditions of the fan to be designed are then:

- achievable maximum volume flow rate $Q_{max}$ = 9500 m$^3$/h;
- total pressure rise $\Delta p_0$ = 550 mm$_{H2O}$ (5394 Pa) @ 8500 m$^3$/h
- rotational speed $n$ = 4050 rpm.

The value of the rotational speed was determined by the usual application of the fan, which is coupled to the truck power take-off. This is connected to the truck shaft engine (which rotates at $n$ = 540 rpm) by means of a 7.5:1 gear-box. Moreover, the manufacturer asked to accomplish with some economic and geometric constraints. These constraints are:

- maximum power lower than 35 CV (25.7 kW);
- as low as possible radial space requirement;
- impeller diameter less than 500 mm;
- as low as possible noise.

The first requirement descended from the truck maximum available power, the second from economic reasons and the third in order to reduce the acoustic load of the mist sprayer/truck systems, which is usually very high and dangerous for operators.

A tentative geometry was defined through geometry correlations as a function of the specific speed $n_c$. In order to meet the above requirements, the analysis revealed that a double entry fan should represent a feasible solution. In this design, the fan is conceived as to be composed by two impeller in parallel arrangement and by a single volute. The partial machines must elaborate half the required volume flow rate but has to supply the total head. As a first estimated according to literature, the efficiency to be used in the subsequent design was evaluated by means of classical statistical correlations: at this stage, the value of this efficiency - very dependent on the source - has only a statistical meaning. A sensitivity analysis revealed that the different values found for the total efficiency, which can range from 0.70 to 0.85, are within a band of about ± 15 %. A literature

survey was first carried out in order to assess the most reliable and most commonly used methods. In particular, the design procedure proposed by Wright [8] and Eck [9], have been analyzed. The preliminary tentative design resulted in an external diameter $D_2$ = 450 mm was then obtained. The impeller eye diameter $D_0$ was estimated by means of the correlation proposed by Wright [8]

$$\frac{D_0}{D_2}=1.53\ \sqrt[3]{\varphi} \qquad (1),$$

where φ is defined by

$$\varphi=\frac{Q'}{ND_2^3} \qquad (2),$$

where $N$ is the rotational speed in round per second, and by means of Eck correlation [9]:

$$\frac{D_0}{D_2}\geq 1.194\ \sqrt[3]{\varphi} \qquad (3)$$

In this case, $\varphi$ is defined as

$$\varphi=\frac{4Q'}{u_2\pi D_2^2} \qquad (4)$$

The blade inlet diameter was chose equal to the impeller eye diameter, i.e. $D_1 = D_0$. Hence, the inlet blade span $b_1$ was chosen according to Eck [14], who proposed the following equation

$$b_1=\frac{D_1}{4\xi} \qquad (5)$$

where $\xi$ is a coefficient which stated if at the blade inlet the meridian velocity should be higher (accelerate), equal or lower (decelerate) with respect to the axial velocity.

Once the main dimensions were chosen, the meridian flow path was designed. To do this the following procedure was adopted. The inlet and outlet velocity ratio can be written as [8]

$$\frac{W_2}{W_1}=\left(\frac{b_1r_1}{b_2r_2}\right)\left(\frac{\sin\beta_1}{\sin\beta_2}\right) \qquad (6)$$

By imposing the meridian velocity distribution in design conditions along the meridian channel, it is possible to calculate the outlet blade span $b_2$.

A very critical parameter is the outlet blade angle $\beta_2^*$. To determine $\beta_2^*$, the relative velocity ratio was chosen according to the well known and established limit proposed by de Haller, which control the diffusion inside the blade passage

$$\frac{W_1}{W_2}>0.72 \qquad (7)$$

With this assumption, it is possible either (i) to calculate the outlet relative flow angle $\beta_2$ by imposing a value for the de Haller ratio or (ii) to impose a realistic value of $\beta_2$ and keep under control if Eq. (7) is satisfied. The outlet blade angle $\beta_2^*$ is then calculated by means of a trial and error procedure which makes use of the slip factor correlation proposed by Stodola [10]

$$C_{\mathrm{H}} = \frac{V_{\mathrm{u2}}}{V_{\mathrm{u2}}^*} = 1 - \frac{\frac{\pi \sin \beta_2^*}{Z}}{1 - \frac{V_{\mathrm{m2}} \cot \beta_2^*}{U_2}} \qquad (8)$$

and the formula for blade number estimation proposed in [9]:

$$z = \frac{4\pi}{1.5} \frac{\sin \beta_2^*}{\left(1 - \frac{r_1}{r_2}\right)} \qquad (9)$$

With this procedure, a number of geometries were generated. The blade mean line was imposed by the manufacturer to be drawn as a single circular arc: this was driven by economic and manufacturing reasons.

## CFD NUMERICAL ISSUES

The numerical simulations were carried out with the commercial CFD code ANSYS CFX 11.0 [11]. The code solves the 3D Reynolds-averaged form of the Navier–Stokes equations by using a finite-element based finite-volume method. A second-order high-resolution advection scheme was adopted to calculate the advection terms in the discrete finite-volume equations. The grids used in the calculations were tetrahedral grids generated by means of ANSYS ICEM CFD 11.0 [12].

The SST *k-ω* two-equation model was used to solve the turbulent flow. Near-wall effects are modeled by means of automatic wall functions [11]. The simulations were performed in steady state conditions. When both stator and rotor are present in the simulation, the simulations are performed in a multiple frame of reference to take into account the contemporary presence of moving and stationary domains. In particular, a mixing plane approach was imposed at the rotor/stator interface. In this approach, a single-pass steady-state solution is calculated exchanging the flow field variables at the interface. Flow field data are averaged circumferentially for both frames of reference at the interface and passed to the adjacent zone as boundary conditions.

## PRELIMINARY CFD DESIGN

### Impeller Design

A first simulation campaign was performed as an initial coarse check on the tentative 1D geometries. The geometries were simulated in a relative frame of references as a single blade without static components (Fig. 2). Hence, only a section of the full geometry has been modeled and, therefore, rotational periodic boundary conditions were applied to the lateral surfaces of the flow domain. A mass flow rate was imposed at the inflow boundary and an average relative static pressure $p_{\mathrm{r2}}$ was imposed at the outflow boundary.

A wide number of impeller geometries (more than 10) were considered for calculations. The results of the most performing ones (reported in Table 1) are analyzed and discussed in details.

The results are reported in Fig. 3. It can be noticed that the three geometries are almost equivalent at design point both with regards to head and to efficiency. It is to underline that, since each impeller has to elaborate half flow rate, the simulations were performed at a flow rate equal to $Q'$ = 4750 $\mathrm{m}^3$/h. As what concern head, the Impeller C seems slightly better than the other two (head at design point almost 10 % higher). By looking at the entire performance curve, Impeller A seems to have a steeper curve, resulting in higher head at low flow rates and lower head at high flow rate.

*Table 1 - One-dimensional geometries*

| Impeller A | | Impeller B | | Impeller C | |
|---|---|---|---|---|---|
| 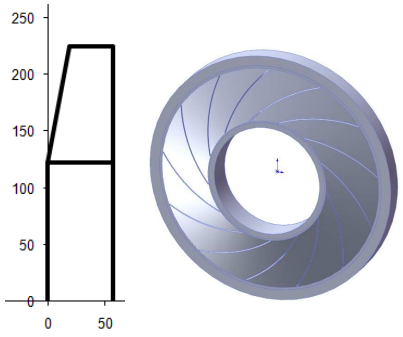 | | 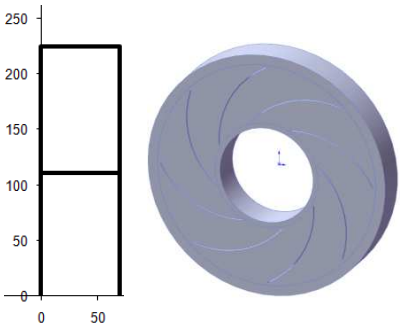 | | 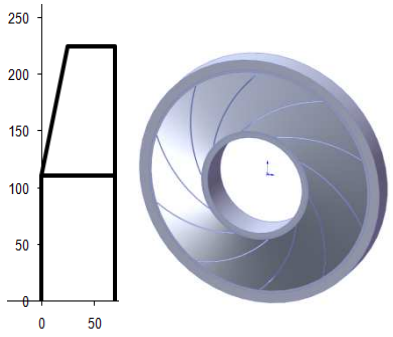 | |
| $z = 13$ | $D_0 = 245$ mm | $z = 8$ | $D_0 = 223$ mm | $z = 10$ | $D_0 = 223$ mm |
| $b_1 = 57$ mm | $b_2 = 38$ mm | $b_1 = 70$ mm | $b_2 = 70$ mm | $b_1 = 70$ mm | $b_2 = 45$ mm |
| $\beta_1^* = 30.0°$ | $\beta_2^* = 40.0°$ | $\beta_1^* = 30.9°$ | $\beta_2^* = 26.5°$ | $\beta_1^* = 31.1°$ | $\beta_2^* = 40.0°$ |

Other significant information can be drawn from the analysis of the efficiency curve. In fact, Impeller A presents a remarkable drop in efficiency at high flow rates and this could result in too high absorbed power in these working points. Some information have been obtained also form the velocity field, depicted in Fig. 4. In fact, the slip factor values calculated for the three impellers by means of Stodola correlation, Eq. (9), were checked against the values obtained from the averaged circumferential velocity $V^*_{u2}$ obtained from the CFD calculations. The Stodola values and the CFD values were found to be in close agreement, thus confirming the correctness of the performed design. Finally, the De Haller ratio was checked in order to fulfill the limit imposed by Eq. (7), both numerically and by looking at the velocity field. As can be seen, no significant separation can be noticed within the blade to blade passages.

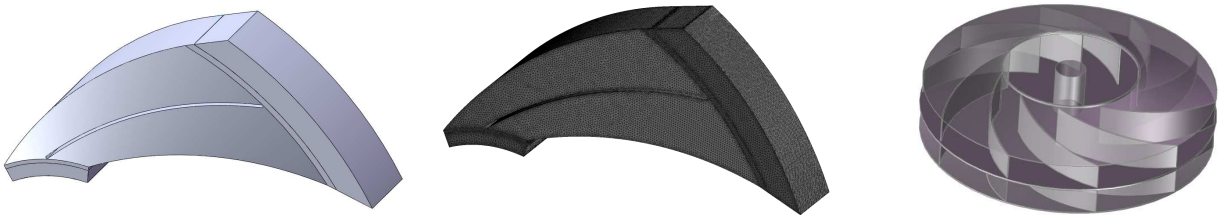

*(a)* *(b)* *(c)*

*Figure 2 - One-dimensional CFD geometries (a), grid (b) and complete Impeller C geometry (c)*

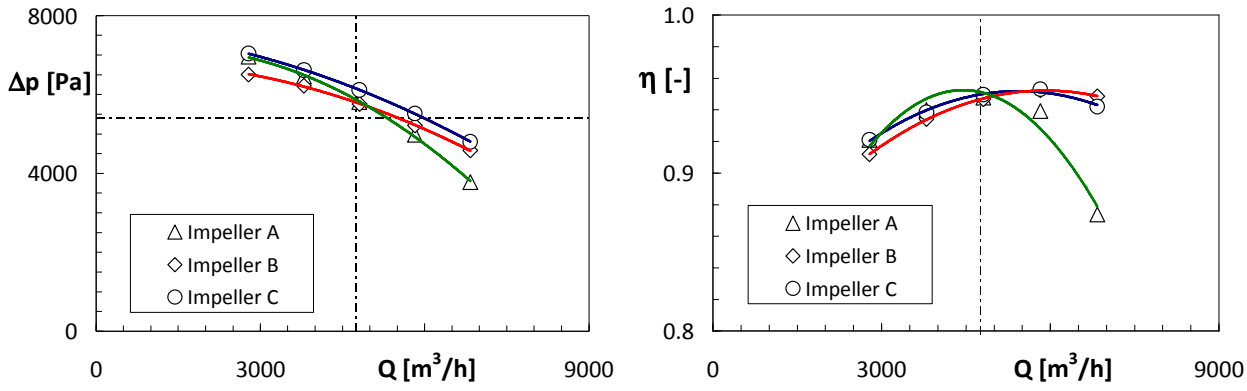


*Figure 3 – Performance curves*

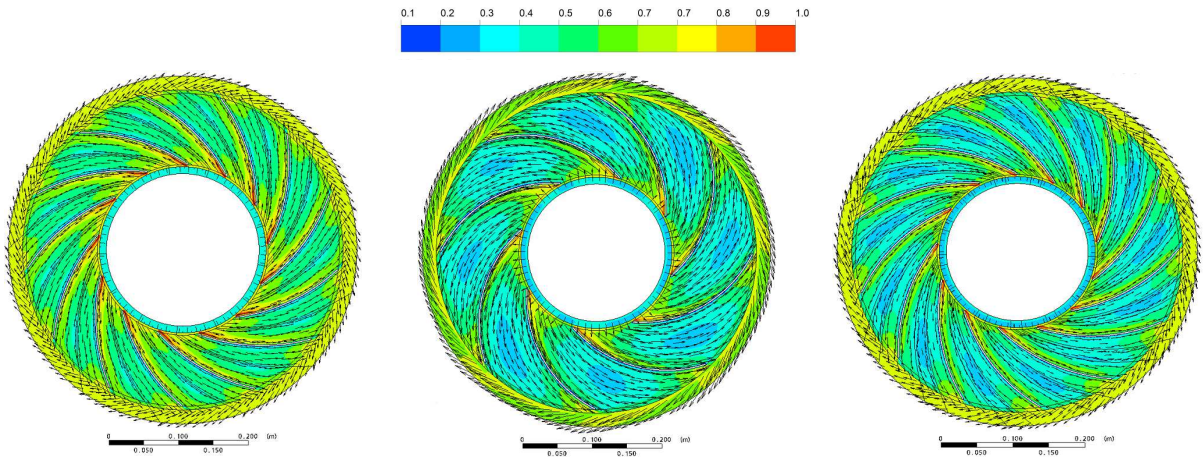


*Impeller A* *Impeller B* *Impeller C*

*Figure 4 – Velocity field (velocity magnitude normalized with maximum velocity)*

As a final result, Impeller C (Fig. 2b) was chosen as candidate geometry for the final fan. However, the head value of the single impeller ($\Delta p$ = 620 $mm_{H2O}$) was considered not from the safe side, since the coupling with the volute and the unavoidable mixing of the two stream arriving from the two impeller in parallel can results in higher than predictable pressure losses.

## Volute Design

The design of the volute was subjected to manufacturing and functional requirements consequent to the particular application under consideration:

- the product (pesticides, etc.) distribution must be performed also at a near distance from the ground. For this reason, some distributors are connected directly to the volute in order to bleed some air in order to feed near-field atomizers (see Fig. 1). As a consequence, an optimized volute design should take into consideration that the volute will operate with a non-constant flow rate;
- to have an as high as possible regular distribution of the flow leaving the volute and to keep an as balanced as possible air distribution in order to equally feed the left and right cannons, the volute outlet flow should be as much as possible regularly developed;
- in order to have a compact and well-balanced assembly, it is preferable to have the volute outlet centered with the fan inlet, i.e a radial discharge volute (goose-neck shaped).

The volute was designed by means of a constant velocity approach, following the Eck [9] and Wright [8] approaches. Three different volute geometries were designed and simulated in conjunction with the Impeller C chosen in the previous phase. At first, a standard tangential volute (sketched in Fig. 5a) was designed and considered as a reference to drive a subsequent correct design. The outlet section dimensions are equal to (209 x 334) $mm^2$.

The standard volute was simulated in order to assess the reference performance to be obtained with the goose-neck volutes. In fact, it has been proved that tangential (standard) and radial (goose-neck) volute present equal merit, if correctly designed.

Moreover, an important information which would have been derived from the simulation is where to allocate the bleed openings, and (i) how much flow rate is expected to leave from the bleed openings for a given distributor geometry or (ii) the area of the bleed openings to guarantee a fixed amount of air flow rate.

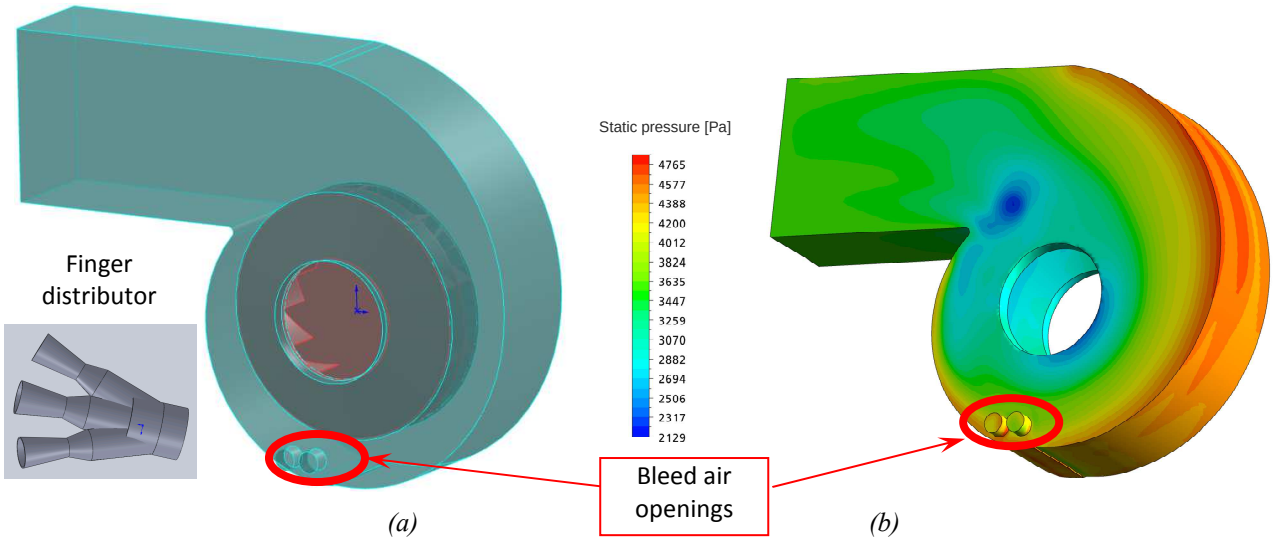


*Figure 5 – Standard volute*

The simulation was performed at the design flow rate $Q$ = 9500 m$^3$/h and at the design rotational speed $n$ = 4050 rpm. At this point, a small sensitivity analysis was performed and grid rationale chosen once for all. A number of tetrahedral grids were generated and a final number of grid points equal to almost 4 000 000 was chosen.

The fan performance resulted equal to $\Delta p$ = 4808 Pa (490.24 mm$_{H2O}$) and $\eta_{in}$ = 0.79. The static pressure field around the volute was then plotted (Fig. 5b). It can be noticed that pressure is quite constant around the external edge of the volute, thus giving confidence that the bleed air openings flow rate would be almost invariant to their position around the volute. To correctly design the openings, a simple one-dimensional lumped parameter pressure drop model for a typical distributor geometry used in these applications (Fig. 5a) has been set up. By applying the inlet pressure boundary conditions derived from the simulation and by assuming ambient pressure at the finger outlet, the expected flow rate at the openings has been derived. The bleed flow rate was calculated equal to 19 % of the total flow rate ($Q_{bleed}$ = 1805 m$^3$/h), which resulted in an average bleed air velocity at the finger outlet equal to 88 m/s. This value was judged to be a little to low to have a correct atomization of the liquid spray and a target value of 100 m/s was fixed. After a trial and error procedure, the air openings position, geometry and flow rate was finally fixed. In particular, following the indications of the pressure field (Fig. 5b), the openings were moved form the side of the volute to the bottom wall. For the subsequent calculations, $Q_{bleed}$ was considered for the design of the volute shape and area variation.

After this phase, two radial discharge geometries are generated: (i) a first goose-neck shaped volute (Fig. 6a, Volute A), in which the volute tongue curvature radius is equal to $r$ = 7 mm and the outlet section has the same dimensions of the standard one; (ii) a second goose-neck shaped volute (Fig. 6b, Volute B), in which the volute tongue curvature radius is equal to $r$ = 22 mm (in order to let the flow approach be more robust to variation in tongue incidence) and the outlet section with dimension as equal to (206 x 286) mm$^2$ (in order to have a less diffusive volute).

**Fan 1# verification**

Two fan composed of a double-entry impeller and a volute were tested by means of the CFD calculation. The two fans are:

- Fan #1-CA, which is composed of Impeller C and Volute A;
- Fan #1-CB, which is composed of Impeller C and Volute B;

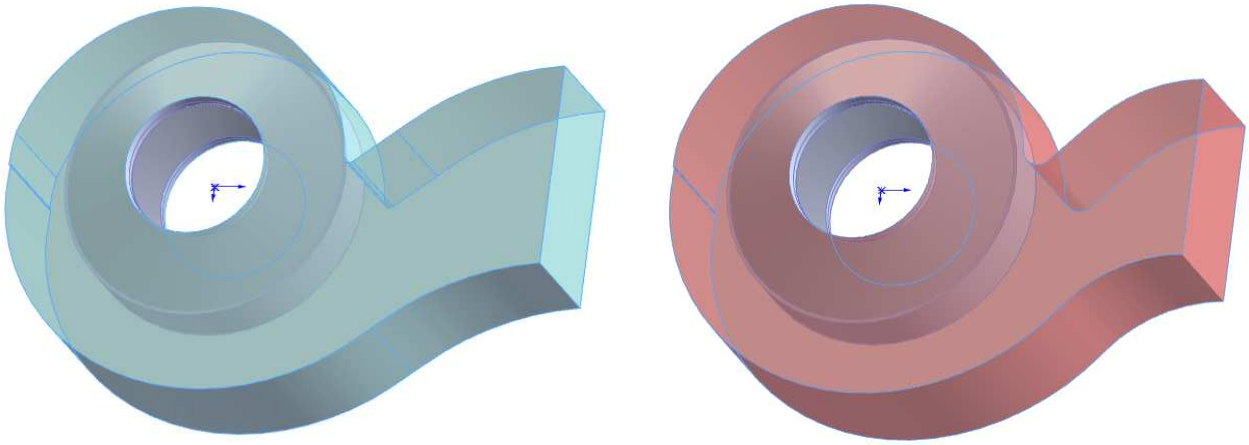

*(a)* *(b)*

*Figure 6 – Radial discharge (goose-neck) volute geometries*

As a reminder, Impeller C has an external diameter $D_2$ = 450 mm. The results in terms of performance parameters are reported in Tab. 2. As can be seen, the three fan geometries have the same internal efficiency (the internal efficiency considers the hydraulic efficiency, the volumetric efficiency and the disk friction efficiency and does not take into account the mechanical and gear box efficiency), thus confirming that the goose-neck shape does not lead to significant efficiency penalty. As what concern head, the predicted values of all these solutions resulted less than the desired one (550 $mm_{H2O}$), as also expected form the preliminary CFD simulations of impeller alone. However, since Volute B seems to perform better than Volute A, the former was used for the final geometry optimization

*Table 2 - Volute performance by means of CFD simulations*

| | Fan #1-CA | Fan #1-CB | Standard |
|---|---|---|---|
| $\Delta p_0$ [Pa] | 4704.3 | 4750.8 | 4807.7 |
| $\Delta p_0$ [$mm_{H2O}$] | 479.7 | 484.4 | 490.2 |
| $P_{abs}$ [kW] | 15.7 | 15.9 | 16.0 |
| $P_{abs}$ [CV] | 21.3 | 21.6 | 21.8 |
| $\eta_{in}$ [-] | 0.79 | 0.79 | 0.79 |

**Fan #2 design and geometry optimization**

As a final step, the Fan #1-CB fan geometry was optimized in order to achieve the expected performance in terms of head and flow field. In fact, although the efficiency seems to reach an acceptable value, the head seems to be still low, even if at a preliminary design. For this reason, two main action were performed:

- the impeller, and consequently the volute, were scaled to an higher diameter in order to fulfill the requested head. From affinity laws, the new tentative diameter was set equal to $D_2$ = 488 mm. The new geometry (Fan #2) take advantage of the previous design phases since the new fan was derived from Impeller C and Volute B coupling. Moreover, the one dimensional procedure was checked by using, during the 1D design procedure, parameters obtained by means of the CFD calculation which were previously chosen by means of statistical correlation and/or experience. These are: (i) the volumetric efficiency, which was estimated equal to $\eta_V$ = 0.94 from Fan#1

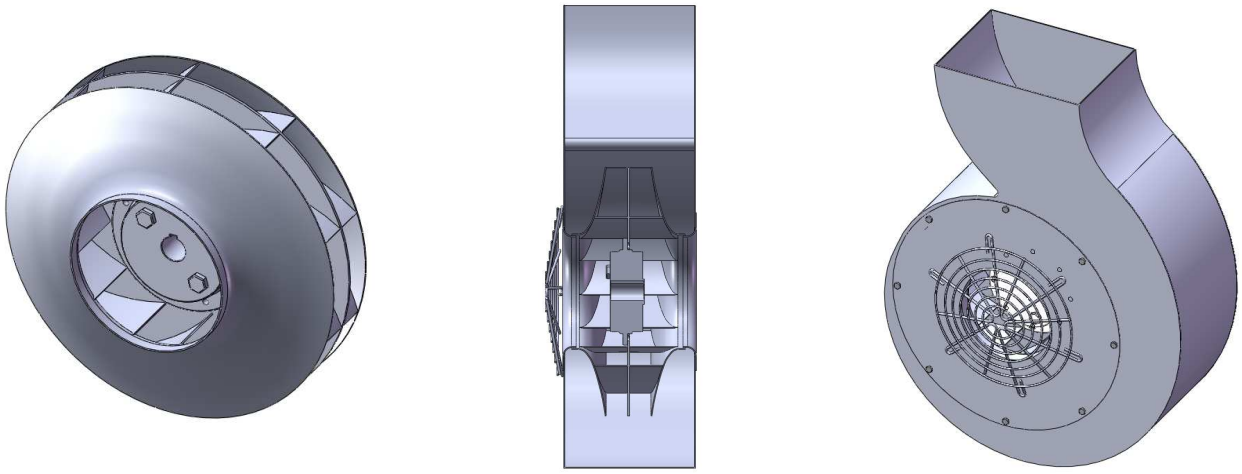

*(a)* *(b)* *(c)*

*Figure 7 – Final geometry: Fan #2*

simulations; (ii) the slip factor, which was checked against Stodola correlation; (iii) the hydraulic and overall efficiency, which were estimated to be $\eta_h = 0.86$ and $\eta = 0.73$, respectively.

- the shroud of Impeller C was redesigned by means of Bezier curves, while the scaled main geometrical dimensions were kept constant. The shroud shape was chosen in order to maintain a linear variation of the meridional velocity (Fig. 7a and 7b).

For the final CFD testing, the geometry was no simplified and devices actually present in the real geometry taken into consideration. In particular: (i) on the left inlet, the presence of a security grid, which is expected to slightly alter the fluid dynamic and to represent a blockage for the inlet flow, was considered; (ii) on the right side (not shown in the Figure) the blockage due to the power shaft was taken into consideration. The designed geometry of Fan#2 is depicted in Fig. 7c.

## EXPERIMENTAL TEST RIG

In order to validate the entire CFD procedure and the Fan#2 geometry effectiveness, an experimental campaign was performed. A test rig (sketched in Fig. 8) was built on purpose.

The rig is composed of a straight pipe connected to the fan by a divergent sector. Since the inlet entry is open to the atmosphere, relative pressure $p_{g1}$ is used to calculate the head of the fan. The pressure $p_{g2}$ and the temperature $T_2$ are used to define the thermodynamic state of the air upstream the orifice plate. Differential pressure transducers with a 0.5 % accuracy were used, while for temperature measurement, a standard T-type thermocouple was used. Ambient conditions in terms of ambient pressure, temperature and relative humidity were recorded by means of a barometric station. The volume flow rate was measured by means of a calibrated orifice plate designed in accordance with the ISO 5167 European standard. The orifice plate has a diameter ratio equal to 0.75 and uses corner taps for the pressure drop $\Delta p_{or}$ measurement, which was performed by means of a 0.3 % accuracy differential pressure transducer. A 19-tube bundle flow straightener, consisting of a bundle of parallel and tangential tubes fixed together and held rigidly in the pipe is used to reduce the length of the pipe upstream of the orifice plate. At the outlet of the tube, a throttling valve is installed allowing the whole operating field to be investigated. Since, the fan is driven by the diesel engine, valve throttling causes a variation of the rotational speed. Therefore, rotational speed is measured for each operating point by a stroboscopic light. The main parameters of the test rig are reported in Tab. 3.

# CFD SIMULATION AND EXPERIMENTAL VALIDATION

As a final step, the final fan geometry Fan#2 was simulated and verified experimentally.

The experimental data were normalized for the standard ambient conditions ($T$ = 15 °C and $p$ = 101325 Pa), and the simulation performed at the same conditions. Since the fan is driven by a diesel engine, valve throttling causes a variation of the rotational speed. The measured points are reported to the same rotational speed by using affinity laws. The chosen rotational speed was equal to $n$ = 4050 rpm. The simulated performance curve was obtained by imposing different value of the static outlet pressure.

As can be seen from Fig. 9a, experimental data and numerical results are in good agreement. The achieved experimental performance were $\Delta p$ = 5373 Pa (548 $mm_{H2O}$) at a flow rate Q = 8540 $m^3/h$, and a maximum achievable flow rate (when coupled to the test circuit) equal to $Q_{max}$ = 10 563 $m^3/h$. Moreover, the pressure distribution along volute is quite constant and confirmed the correctness of the volute design. Hence, the initial requirement were substantially achieved, and, thus, the design frozen (Fig. 9b).

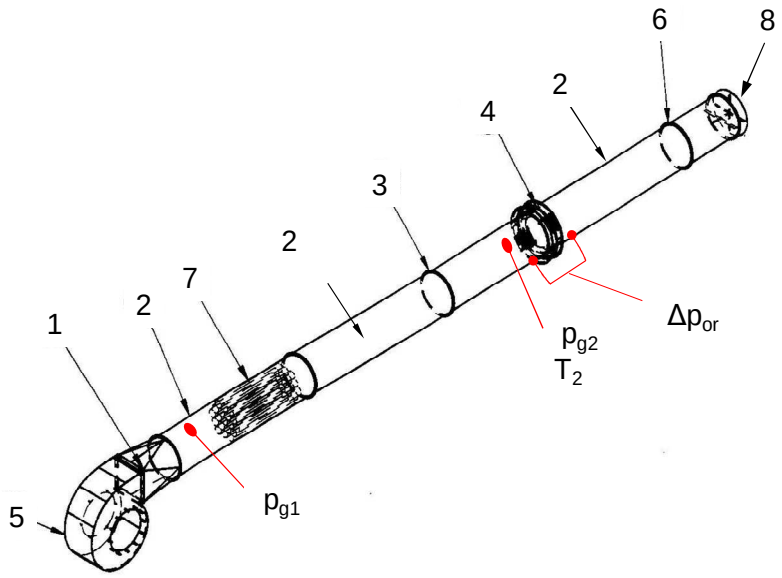


*Figure 8: Test rig and sensor positions*

*Table 3: Main features of the test rig*

| | | *L* [m] | *D* [m] |
|---|---|---|---|
| 1 | conical adaptor | 1.032 | - |
| 2 | circular duct | 0.520 | 0.520 |
| 3 | circular duct | 6.024 | 0.520 |
| 4 | orifice plate | - | 0.390 |
| 5 | fan | - | - |
| 6 | circular duct | 2.600 | 0.520 |
| 7 | flow straightener | 1.040 | 0.502 |
| 8 | throttling valve | - | 0.520 |

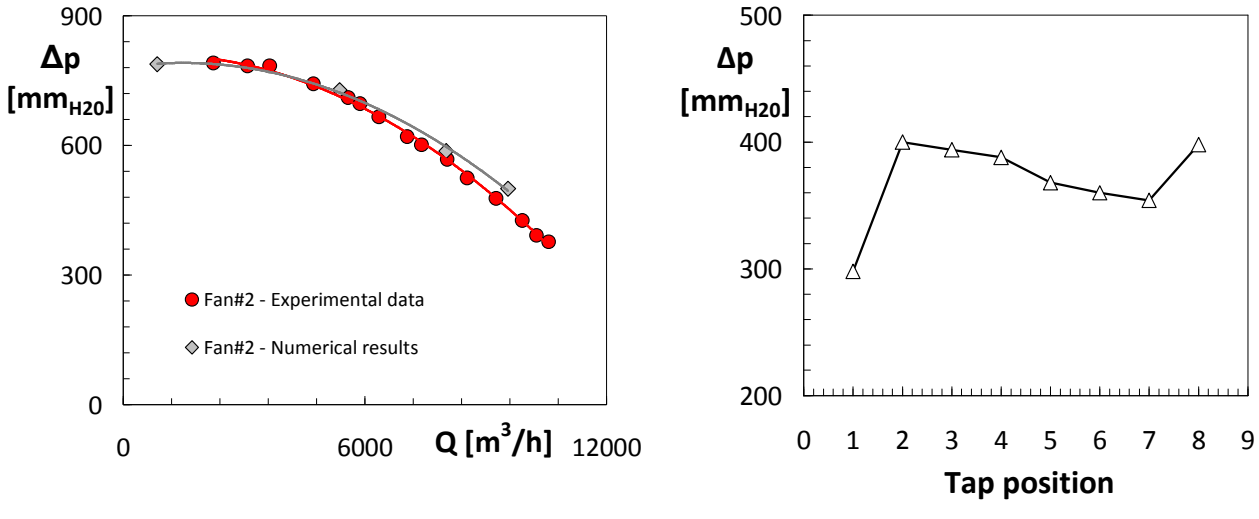


*(a)* *(b)*

*Figure 9: Numerical and experimental Fan#2 performance (a) and pressure around volute@9600 $m^3/h$ (b)*

*Figure 10: Final geometry*

# BIBLIOGRAPHY

[1] Gan-Mor, S., Matthews, G.A., **2003**, *Recent Developments in Sprayers for Application of Biopesticides: an Overview*, Biosystems Engineering, 84(2).

[2] Hoffmann, W.C., Walker, T.W., Martin, D.E., Barber, J.A., Gwinn, T., Smith, V.L., Szumlas, D., Lan, Y., Fritz, B.K., **2007**, *Characterization of truck-mounted atomization equipment typically used in vector control*, J. Am. Mosq. Control Assoc., 23(3), pp. 321-329.

[3] Bettocchi, R., Morini, M., Pinelli, M., **2011**, *Evaluation of the performance of a sirocco fan driven by a diesel engine in mist sprayer applications,* ASME Paper GT2011-45539.

[4] Ferrari, C., Pinelli, M., Spina, P. R., Bolognin, P., Borghi, L., **2011**, *Fluid dynamic design and optimization of two stage high performance centrifugal fan for industrial burners, ASME Paper GT2011-46087.*

[5] Ng, W.K., and Damodaran, M., **2006**, *Computational flow modeling for optimizing industrial fan performance characteristics*, European Conference on Computational Fluid Dynamics, ECCOMAS CFD 2006, P. Wesseling, E. Oñate, J. Périaux (Eds), Paris

[6] Lee, Y.T., Ahuja, V., Hosangadi, A., Slipper, M.E, Mulvihill, L.P., Birkbeck, R. and. Coleman, R., **2011**, Impeller *Design of a Centrifugal Fan with Blade Optimization*, International Journal of Rotating Machinery, 537824, pp 1-16

[7] Tallgren, J.A., Sarin, D.A., Sheard, A.G., **2004**, *Utilization of CFD in development of centrifugal fan aerodynamics,* C631/016/2004, Proc. Int. Conf. on Fans, IMEChE Publishing.

[8] Wright, T., **1999**, *Fluid machinery-Performance, analysis and design*, CRC Press.

[9] Eck, B., **1973**, *Fans*, Pergamon Press, New York.

[10] Stodola, A., **1945**, *Steam and Gas Turbines*, McGraw-Hill, New York.

[11] ANSYS CFX 11.0, **2007**, *User Manual*.

[12] ICEM CFD 11.0, **2007**, *User Manual.*